RSC Mechanochemistry

ROYAL SOCIETY OF CHEMISTRY

PAPER

View Article Online
View Journal | View Issue

Cite this: *RSC Mechanochem.*, 2024, **1**, 520

Mechanochemical synthesis of fluorinated perovskites $KCuF_3$ and $KNiF_3$†

Davide Ceriotti, [a] Piergiorgio Marziani, [a] Federico Maria Scesa, [a] Arianna Collorà, [a] Claudia L. Bianchi, [bc] Luca Magagnin [ad] and Maurizio Sansotera [*ad]

Received 19th April 2024
Accepted 23rd August 2024

DOI: 10.1039/d4mr00037d

rsc.li/RSCMechanochem

A solvent-free mechanochemical synthesis of two fluorinated perovskites, $KCuF_3$ and $KNiF_3$, including the optimization of milling time at constant rotational speed, was studied as a practical and green alternative to the classical solvothermal synthesis. The presence of $KCuF_3$ and $KNiF_3$ in the desired crystalline phase as the main product was observed after 6 h of milling. At higher milling times K_2CuF_4 and K_2NiF_4 were detected as additional crystalline phases for the Cu- and Ni- based perovskites, respectively. The fluorinated perovskites were characterized by using X-Ray Powder Diffraction (XRD), X-Ray Photoelectron Spectroscopy (XPS) and Scanning Electron Microscopy (SEM), confirming the selective formation of the fluorinated perovskites. The mechanochemical route was also compared to a new mild solvothermal method. An evaluation of the environmental impact and the energy efficiency was performed; moreover, the effectiveness of the mechanochemical process was compared to that of the solvothermal method. The promising results obtained from this innovative method opened the door to the use of solvent-free mechanochemical syntheses as a suitable approach in the field of crystal engineering also.

Introduction

Perovskites are an emerging class of semiconducting materials with tunable bandgaps, wide color gamut, high charge-carrier mobilities, and long carrier diffusion lengths.[1,2] They are usually characterized by a generic formula ABX_3 where A and B are metal cations, while X is generally an anion.[3,4] In metal halide perovskites, A is a monovalent cation (*e.g.*, Na^+, Cs^+, and K^+), B is a divalent transition metal cation (*e.g.*, Mg^{2+}, Cu^{2+}, Ca^{2+}, Ni^{2+}, Pb^{2+}, and Cu^{2+}), and X is a halide monovalent anion (*e.g.*, I^-, Cl^-, and F^-). The traditional crystal structure of halide perovskites, ABX_3, is characterized by $[MX_6]^{4-}$ octahedra that share corners in all three orthogonal directions to produce endless three-dimensional (3D) $[MX_3]$ frameworks.[5] In the recent decades, fluorine-based cubic perovskites have been studied because of their intriguing features like high temperature superconductivity,[6] as well as their electrical,[7] optical[8] and magnetic properties.[9] Among fluorinated perovskites, $KNiF_3$ has a typical ABX_3 octahedral structure with a cubic unit cell with a NiF_6 octahedron, where the K^+ ions fill the empty spaces within the octahedron itself.[10] $KNiF_3$, as a pure compound or in CNTs nanocomposites, has been used as an electrode material in supercapacitors[11] introducing different bimetallic elements in order to realize the optimal synergistic effect, which largely contributed to specific capacity and rate capability of the material.[12] $KCuF_3$ has a different structure mainly due to Jahn–Teller effects[13] and it is characterized by distorted octahedra, where the Cu–F bonds have different lengths because of the displacement of F^- ions on the *c* plane of the Cu–F–Cu bonds.[14,15] $KCuF_3$ found applications as a cost-effective anode in lithium-dual-ion batteries.[16] Both fluorinated perovskites, $KNiF_3$ and $KCuF_3$, were employed in the formation of artificial solid electrolyte interfaces (SEIs) for obtaining air-stable and dendrite-free lithium metal anodes.[17]

The physical and electrical properties of fluorinated perovskites are largely dependent on their synthesis because it significantly affects their dimension and shape; thus, several methods were developed: the conventional solid state reaction at high temperature,[18] hydrothermal processes,[19,20] and microemulsion-based methods.[21] Mechanochemical synthesis of perovskites has emerged in recent years as a viable alternative to traditional chemical syntheses, spanning applications from organic–inorganic hybrid materials to fully inorganic perovskite-type electro-ceramics.[22] This method has rapidly gained recognition as an environmentally friendly route for

[a]*Dipartimento di Chimica, Materiali e Ingegneria Chimica, Politecnico di Milano, via Mancinelli 7, 20131 Milano, Italy*

[b]*Dipartimento di Chimica, Università degli Studi di Milano, via Golgi 19, I-20133 Milano, Italy*

[c]*Consorzio Interuniversitario Nazionale per la Scienza e Tecnologia dei Materiali (UdR – UniMi), via G. Giusti, 9, 50121 Firenze, Italy*

[d]*Consorzio Interuniversitario Nazionale per la Scienza e Tecnologia dei Materiali (UdR– PoliMi), via G. Giusti, 9, 50121 Firenze, Italy. E-mail: maurizio.sansotera@polimi.it; Fax: +39 2 2399 3280; Tel: +39 2 2399 4770*

† Electronic supplementary information (ESI) available. See DOI: https://doi.org/10.1039/d4mr00037d

chemical modification in materials science, particularly in electronics, optoelectronics,[23] and electrochemical fields.[24,25] Utilizing mechanical forces in a one-step process,[26] typically through high-energy ball milling, this approach facilitates reactions without hazardous, expensive, or polluting solvents. It offers a sustainable alternative to high-temperature, solution-based synthesis, and the potential of this technique is demonstrated in tailoring the properties of final products by manipulating reaction conditions such as milling energy, reaction time, stoichiometry, or additive insertion.[27,28]

In this work, the mechanochemical syntheses of $KNiF_3$ and $KCuF_3$ were described and compared to a mild solvothermal synthesis performed at mild temperature in a relatively fast process. A planetary instrument was employed for the mechanochemical reactions: in a planetary ball mill, the collisions between the milling media and the treated materials were generated by the simultaneous rotation of the base plate and the jar; these impacts were responsible for producing the necessary kinetic energy for the reaction, allowing the conversion of the starting materials.[29] The yield of the reaction was strictly dependent on the selected milling parameters, which included the rotational speed, media filling ratio, powder filling ratio and milling time. The first three parameters directly influenced the kinetic energy of the spheres, modifying their speed, directly in the case of the rotational speed, or indirectly in the case of media filling ratio and powder filling ratio influencing the free space available inside the jar that the spheres required to gain velocity and, thus, kinetic energy, before the impact. The milling time enhanced the probability that the kinetic energy released by the impacts was exploited for the reaction rather than being dissipated as heat or against the walls of the jar. The parameters employed in the mechanochemical syntheses were discussed and the properties of the perovskites, such as their crystalline phases, compositions, and morphologies, were also reported.

This work also evaluates whether the mechanochemical process is actually more environmentally friendly than the solvothermal process from both a chemical and energetic point of view. Some green metrics commonly used in these cases were examined:[30] the theoretical atom economy of the process (AE) and the theoretical process mass intensity (PMI).

$$\mathrm{AE} = \frac{\text{molecular weight product } \left(\mathrm{g\ mol^{-1}}\right)}{\text{molecular weight of all reactant used } \left(\mathrm{g\ mol^{-1}}\right)} \times 100$$

$$\mathrm{PMI} = \frac{\text{total mass used in the process(g)}}{\text{mass of the product (g)}}$$

The atom economy evaluates a synthetic process *a priori* and it reveals a low environmental impact when the maximum number of reactant atoms are found in the products. Therefore, the fewer by-products created in a process, the more efficient it is. Process mass intensity is defined as the total mass (including reagents, solvents, catalysts, *etc.*), expressed in grams, of raw materials used to synthesize 1 gram of the product. It is a parameter that must be determined *a priori*, similar to the atom economy. When comparing two processes, a lower PMI value usually indicates a lower environmental impact.[31]

These metrics emphasise the importance of avoiding the use of unnecessary solvents, or the huge amounts of waste produced in some syntheses. When designing a mechanochemical process, these parameters must be taken into account in order to achieve the desired result with the least possible waste of resources.

Furthermore, the energy consumption required for perovskite synthesis by mechanochemical and solvothermal methods was evaluated, using as a reference the maximum theoretical quantity that can be synthesized with the corresponding equipment. In this way, it is possible to observe whether the use of mechanical energy can be a valid alternative to thermal energy also from an energy point of view, as it has been demonstrated in numerous studies for other chemical syntheses.[32]

The actual yields of the reactions were not considered for these evaluations as they depend on the optimization of the process, which, in the solvothermal case, was not performed.

Materials and methods

Materials

Potassium fluoride (KF), nickel chloride hexahydrate ($NiCl_2 \cdot 6H_2O$), nickel fluoride (NiF_2), copper chloride ($CuCl_2$) and copper fluoride (CuF_2) were purchased from Sigma Aldrich as ACS reagent grade of >99.0% purity. The compounds were vacuum dried at 120 °C for 24 h to eliminate possible hydration water and humidity.

Methodology

The mechanochemical reactions were performed under standard conditions (25 °C, 1 atm) inside a planetary ball mill (High Speed Planetary Ball Mill, TOB-ZQM Series, "TOB NEW ENERGY") at 350 rpm rotational speed. The media filling ratio and powder filling ratio were directly related to the diameter and the number of spheres used as milling media, the volume of the jar and the volume of the inlet materials.[33] The media filling ratio (γ_{media}), in particular, is the ratio of the volume of the milling media, including free spaces, to the volume of the chamber, whereas the powder filling ratio (γ_{powder}) is the ratio of the volume of the powder bulk to the volume of the free spaces among the milling media.

$$\gamma_{\mathrm{media}} = \frac{V_{\mathrm{media,bulk}}}{V_{\mathrm{chamber}}}$$

$$\gamma_{\mathrm{powder}} = \frac{V_{\mathrm{powder,bulk}}}{V_{\mathrm{free\ space}}}$$

In the literature, optimal values are reported between 0.3 and 0.5 for the media filling ratio and between 0.5 and 1.0 for the powder filling ratio.[34]

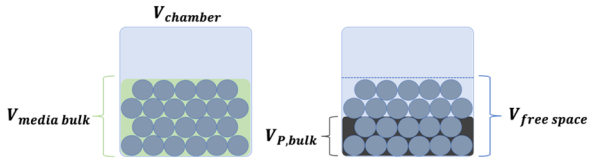

Fig. 1 Graphical representation of the media filling ratio (on the left) and the powder filling ratio (on the right).

The visual representation of the media filling ratio and powder filling ratio is shown in Fig. 1.[33]

Every sample was synthetized in a 50 mL zirconia jar with a defined number of zirconia grinding balls: 39 balls of 8 mm diameter. An equimolar amount of KF and CuF_2 or NiF_2 were weighted according to Table 1 and placed inside the zirconia jar.

The two-steps milling procedure included 15 minutes clockwise and 15 minutes anti-clockwise rotation with 1 minute of resting time between the two steps. The rest was performed in order to avoid temperature increases that can affect the results and could potentially damage the instrument. Three different grinding times were defined: 3 h, 6 h and 12 h (including the rest).

The solvothermal method was performed for both $KNiF_3$ and $KCuF_3$, following the same procedure: KF was dissolved in a minimal amount of distilled water (4/5 mL) while nickel or copper chloride were dissolved in 40 mL of ethanol according to the data present in Table 2. The two solutions were then mixed together in a Teflon® reactor and placed inside a stainless steel (AISI 316) autoclave. The reaction was performed at 185 °C for 16 h. At the end of the thermal step, the resulting precipitate was filtered and washed first with pure ethanol and then with a mixture 80/20 (v/v) of ethanol and water three times. The final product was dried under vacuum at 90 °C for 12 h.

Characterization techniques

The final products were characterized by X-Ray Powder Diffraction (XRD) (Philips PW 1830) using a Bragg Brentano diffractometer and Cu-Kα_1 radiation ($\lambda = 0.154056$ nm) from 5° to 70°, at 1° min^{-1}, with a step size $[2\theta] = 0.0260°$ to identify the $KCuF_3$ and $KNiF_3$ structure and to verify the presence of unreacted reagents or different crystalline phases produced. In order to assess the effect of milling time increase on crystallite size, the crystallites diameters were evaluated with the Scherrer equation:[35]

$$\tau = \frac{K\lambda}{\beta \cos\theta}$$

where τ is the average diameter of the crystallites, K is a dimensionless shape factor equal to 0.9, λ is the wavelength of the Cu-Kα_1 radiation of 0.154056 nm, β is the line broadening at half the maximum intensity (FWHM) in radians and θ is the Bragg angle in radians. Rietveld refinements were employed to identify and quantify the different crystalline phases. The goodness of fit was assessed by using the weighted profile R-factor (R_{wp}).

Table 1 Mechanochemistry reagents employed

Sample	KF	CuF_2	NiF_2
$KCuF_3$	0.730 g (12.5 mmol)	1.27 g (12.5 mmol)	—
$KNiF_3$	0.750 g (12.9 mmol)	—	1.25 g (12.9 mmol)

Table 2 Solvothermal reagents employed

Sample	KF	$CuCl_2$	$NiCl_2 \cdot 6H_2O$
$KCuF_3$	0.261 g (4.5 mmol)	0.201 g (1.5 mmol)	—
$KNiF_3$	0.174 g (3.0 mmol)	—	0.236 g (1.0 mmol)

Scanning Electron Microscopy (SEM) and quantitative Energy Dispersive X-ray Spectroscopy (EDS) were also performed to evaluate the shape and the morphology of the particles and the possible content of other chemical species as impurities.

X-Ray Photoelectron Spectroscopy (XPS) was performed to confirm the XRD results. XPS was conducted using an M-probe apparatus (Surface Science Instruments). The source was a monochromatic Al Kα radiation (1486.6 eV). A spot size of 200 × 750 μm and a pass energy of 25 V were used. Fits were performed using pure Gaussian peaks and Shirley's baseline, without any constraints. Survey and high-resolution spectra have been obtained to determine the compositions of the samples and the oxidation states of the elements. By fitting the C 1s signal, the main peak has been shifted in order to set the adventitious carbon peak at 284.6 eV. C 1s, Ni 2p, O 1s, F 1s and K 2p has been recorded for $KNiF_3$ and C 1s, Cu 2p, O 1s, F 1s and K 2p for $KCuF_3$. The peaks in high resolution XPS spectra were assigned according to literature data on fluorinated perovskites.[15,22,24] XPS errors on the measurements were evaluated considering the atomic scaling factors (ASFs) of the elements detected.

Results

The fluorinated perovskites were synthesized with a solid-state reaction by using the mechanochemical procedure. Three tests were performed at different milling times: 3 h, 6 h and 12 h with a rotational speed of 350 rpm, media filling ratio equal to 0.5 and powder filling ratio fixed at 0.5. KMF_3-structured perovskites are the most prevalent crystalline species obtained, following the reactions:

$$KF + CuF_2 \xrightarrow[\text{kinetic energy}]{\therefore} KCuF_3$$

$$KF + NiF_2 \xrightarrow[\text{kinetic energy}]{\therefore} KNiF_3$$

After 12 hours of milling, the occurrence of K_2MF_4 side crystals as a product of subsequent KF addition to the perovskite structure was observed. Indeed, as the reaction time increases, the mechanochemical forces generated by the interactions between the milling media and the treated materials

result in the build-up of more intense mechanical stresses; these higher mechanical stresses promote reactions that may not occur under conventional synthesis conditions. This phenomenon applied to the milling conditions employed lead to the minor formation of K_2CuF_4 and K_2NiF_4,[36] as additional crystalline species.

The solvothermal method was performed at high temperatures (*i.e.*, 185 °C) with ethanol in an autoclave, by following a different reaction pathway that included the production of KCl as a by-product:

$$3KF + CuCl_2 \xrightarrow[EtOH]{\Delta} 2KCl + KCuF_3$$

$$3KF + NiCl_2 \xrightarrow[EtOH]{\Delta} 2KCl + KNiF_3$$

The perovskites were easily separated from KCl with a final filtration step, exploiting their low solubility in water and ethanol.

XRD results

The XRD patterns of the fluorinated perovskites produced at different milling times (*i.e.*, 3 h, 6 h and 12 h) were compared to those synthetized through the solvothermal method. In the XRD pattern of $KCuF_3$ samples, shown in Fig. 2, the presence of the crystalline phase of the corresponding fluorinated perovskite was observed in accordance with its XRD standard card (JCPDS: 730233).[37] At 3 h the peaks attributed to copper difluoride, CuF_2, were still present and, therefore, the reaction was not yet quantitatively completed. At 6 h CuF_2 peaks disappeared, suggesting that the completeness of the reaction was reached. Signals ascribable to the growth of the K_2CuF_4 crystalline phase were also detected at 12 h of milling time.

In the mechanochemical syntheses of $KNiF_3$ (Fig. 3), the precursors of the perovskite successfully reacted because the crystalline phases of KF or NiF_2 were not detected in the XRD pattern of the products, although their presence as an amorphous phase cannot be excluded. The synthesis of $KNiF_3$ was confirmed in accordance with the XRD standard card of $KNiF_3$ (JCPDS: 21-1002), and the peaks associated with the cubic crystalline phase of $KNiF_3$ were clearly visible.[12] In the samples of $KNiF_3$ produced by mechanochemical syntheses, an additional crystalline phase ascribable to the presence of K_2NiF_4 was observed: these peaks were almost negligible after 3 h, but they became more relevant by increasing the milling time to 6 h and to 12 h.

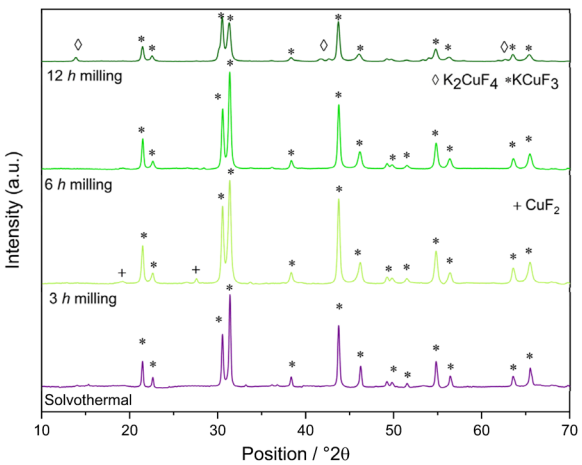

Fig. 2 Powder XRD pattern of $KCuF_3$ samples.

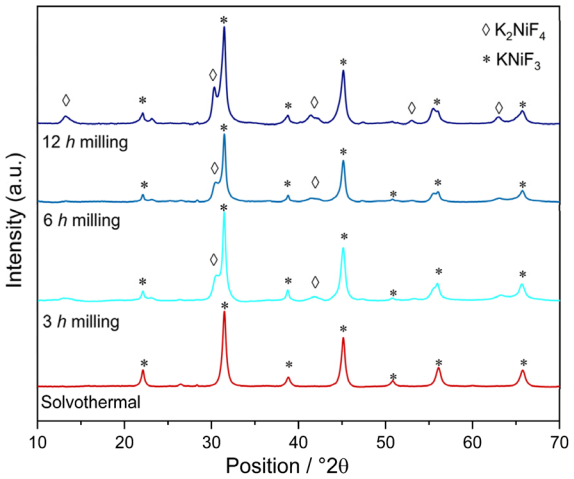

Fig. 3 Powder XRD pattern of $KNiF_3$ samples.

The quantification of the different crystalline phases obtained by the Rietveld refinement is presented in Table 3 and 4. The original XRD patterns with the quantification of each peak are shown in the ESI.†

In the case of $KCuF_3$ perovskites, after 6 h of milling a quantitative formation of the product without side-products was observed. In the case of the Ni-based samples, at 3 h of milling the highest production of $KNiF_3$ was observed and at longer times the formation of a greater quantity of the K_2NiF_4 phase was detected. For both the perovskites it was confirmed that the higher the milling time, the higher the content of K_2CuF_4 and K_2NiF_4, respectively. The examination of the crystallite diameters with the Scherrer equation revealed a decrease,

Table 3 Quantitative results of $KCuF_3$ crystalline phases

Phase	Solvothermal	Milling 3 h	Milling 6 h	Milling 12 h
$KCuF_3$	100%	98.5%	100%	80%
K_2CuF_4	—	—	—	20%
CuF_2	—	1.5%	—	—

Table 4 Quantitative results of $KNiF_3$ crystalline phases

Phase	Solvothermal	Milling 3 h	Milling 6 h	Milling 12 h
$KNiF_3$	100%	84%	70%	65%
K_2NiF_4	—	16%	30%	35%

Table 5 Scherrer diameters of the crystallites (expressed in nm)

Sample	Solvothermal	3 h milling	6 h milling	12 h milling
$KCuF_3$	37	29	28	25
$KNiF_3$	17	15	14	12

albeit minimal, in the average size of the crystallites as the milling hours increased (Table 5).

XPS results

XPS survey analyses measured the elemental composition of the surface of the two perovskite samples obtained by mechanochemical (6 h and 12 h of milling time) and solvothermal syntheses. According to the nominal formula of the perovskite fluorides (ABF_3), the expected atomic composition of the samples was 20% for "A" the monovalent cation (K^+), 20% for "B" the divalent cations (Cu^{2+} and Ni^{2+} respectively) and 60% for the sum of the remaining three monovalent fluorine anions (F^-). In particular, the atomic percentage of the main components for the copper-based fluorinated perovskites (Table 6) resulted in agreement with the theoretical composition of $KCuF_3$: a fluorine content equal to 56% was detected for the mechanochemical procedure lasting 6 h, 60% after 12 h and 64% in the specimen obtained by solvothermal synthesis. For the 6 h procedure, potassium and copper showed the same quantity of 22%; conversely, the other two syntheses induced slightly lower copper contents in favor of the potassium contents: after 12 h of mechanochemical synthesis Cu and K were 16% and 24%, respectively; in the solvothermal sample Cu and K were 13% and 21%, respectively. Therefore, the K : Cu atomic ratio was 1 : 1 and 1 : 1.5 in the 6 h and 12 h syntheses, respectively, and 1 : 1.6 in the solvothermal sample. These slight differences, compared to the theoretical composition, could be confirmed by the species found in the deconvolutions obtained in the high-resolution spectra of these three elements (Fig. 4). The presence of marginally greater amounts of K and F atoms than the theoretical values, can be explained, in fact, by the presence of unreacted KF or by the formation of the K_2CuF_4 crystalline phase.

In potassium high-resolution spectra, the $KCuF_3$ $2p_{3/2}$ peak was detected at 293.5 eV and 293.7 eV in the samples milled for 6 h and 12 h, respectively. These signals were in agreement with the 293.6 eV peak of the solvothermal synthesis, in which KCl formation in little amounts can be noticed due to the peak at 295.9 eV.[38,39] The peak at 294.1 eV was assigned to the $2p_{3/2}$ signal of residual KF in the sample milled for 6 h.[38,40] After 12 h of milling, the formation of a crystalline phase due to K_2CuF_4 was detected by XRD measurement and the XPS signal at 294.5 eV can be ascribed to the presence of this compound. The high resolution spectra in the Cu region showed trends which were in agreement with the deconvolutions observed for potassium signals: after 6 h of mechanochemical synthesis two Cu $2p_{3/2}$ peaks were evident at 933.9 eV and 937.2 eV and they can be assigned to $KCuF_3$ and CuF_2, respectively;[41] after 12 h, $KCuF_3$ was observed in a similar range at 933.4 eV and a signal due to K_2CuF_4 was observed at 939.4 eV; in the solvothermal sample the perovskite peak was at 934.0 eV and the formation of a small amount of CuF_2 was confirmed by the appearance of a peak at 937.4 eV.[41] The high resolution analyses in the F 1s region confirmed the presence of the chemical species detected in the other spectra: after 6 h of mechanochemical synthesis three bonds of a different nature were observed at 683.4 eV, 684.6 eV and 686.2 eV, and they were ascribable to KF, CuF_2 and $KCuF_3$, respectively;[41] after 12 h, CuF_2 reacted quantitatively with KF, the partial formation for K_2CuF_4 was detected and, therefore, only the signals at 686.2 eV of $KCuF_3$ and at 684.1 eV due to K_2CuF_4 were observed;[41] in the solvothermal synthesis, the peak at 686.2 eV due to $KCuF_3$ was clearly present.

In $KNiF_3$ samples, the contents of K, F and Ni atoms were measured by XPS survey analyses and they were mainly in agreement with the theoretical composition of a Ni-based perovskite (Table 7): F contents were 56%, 57% and 60% after 6 h and 12 h of the milling procedure and in the solvothermal sample, respectively, and, therefore, these quantities were approximately in agreement with the expected values; K contents were 26%, 29% and 20%, respectively, and it should be noticed that the mechanochemical procedures induced potassium contents slightly higher that what is theoretically expected; Ni contents were complementary to the other data and, thus, the nickel amount in the sample obtained by 12 h milling decreased to 14% while it was around 18% for both the 6 h milling and the solvothermal samples. These differences from the theoretical values can be explained by the presence of K_2NiF_4, especially after 12 h of the milling procedure. The chlorine content in the solvothermal sample was due to a little amount of KCl that was undissolved by the washing procedure.

The deconvolutions of the K 2p, Ni 2p and F 1s high resolution XPS spectra are shown in Fig. 5 and they confirmed the formation of $KNiF_3$, showing slight amounts of by-products. The K 2p spectrum of the sample synthetized by 6 h milling showed a broad peak centered at 293.0 eV with a shoulder signal at around 295.9 eV which can be attributed to the $KNiF_3$, in particular to a $2p_{3/2}$ and $2p_{1/2}$ doublet due to the spin-orbit coupling typical for K.[42] The binding energy split of these two signals resulted in agreement with the typical energy difference of K of around 2.8 eV.[41] In the literature, K signals of KF were reported in the range from 292.1 to 293.2 eV and these were in agreement with the peaks observed in the experimental spectra, confirming the presence of little amounts of KF in all the samples.[40,43] Indeed, the peaks related to the perovskite were accompanied by a doublet at 293.2 and 296.0 eV coming from KF excess coming from the unconverted reagents. A similar K 2p spectrum was recorded for the solvothermal sample with the main peaks of $KNiF_3$ at 293.5 ($2p_{3/2}$) and 296.4 eV ($2p_{1/2}$) and

Table 6 Atomic composition by XPS analysis of $KCuF_3$ samples

Sample	Potassium at%	Copper at%	Fluorine at%
6 h milling	22.0 (±0.3)	22.0 (±1.1)	56.0 (±0.6)
12 h milling	23.8 (±0.3)	15.6 (±0.7)	60.6 (±0.6)
Solvothermal	20.7 (±0.3)	13.0 (±0.6)	64.3 (±0.7)

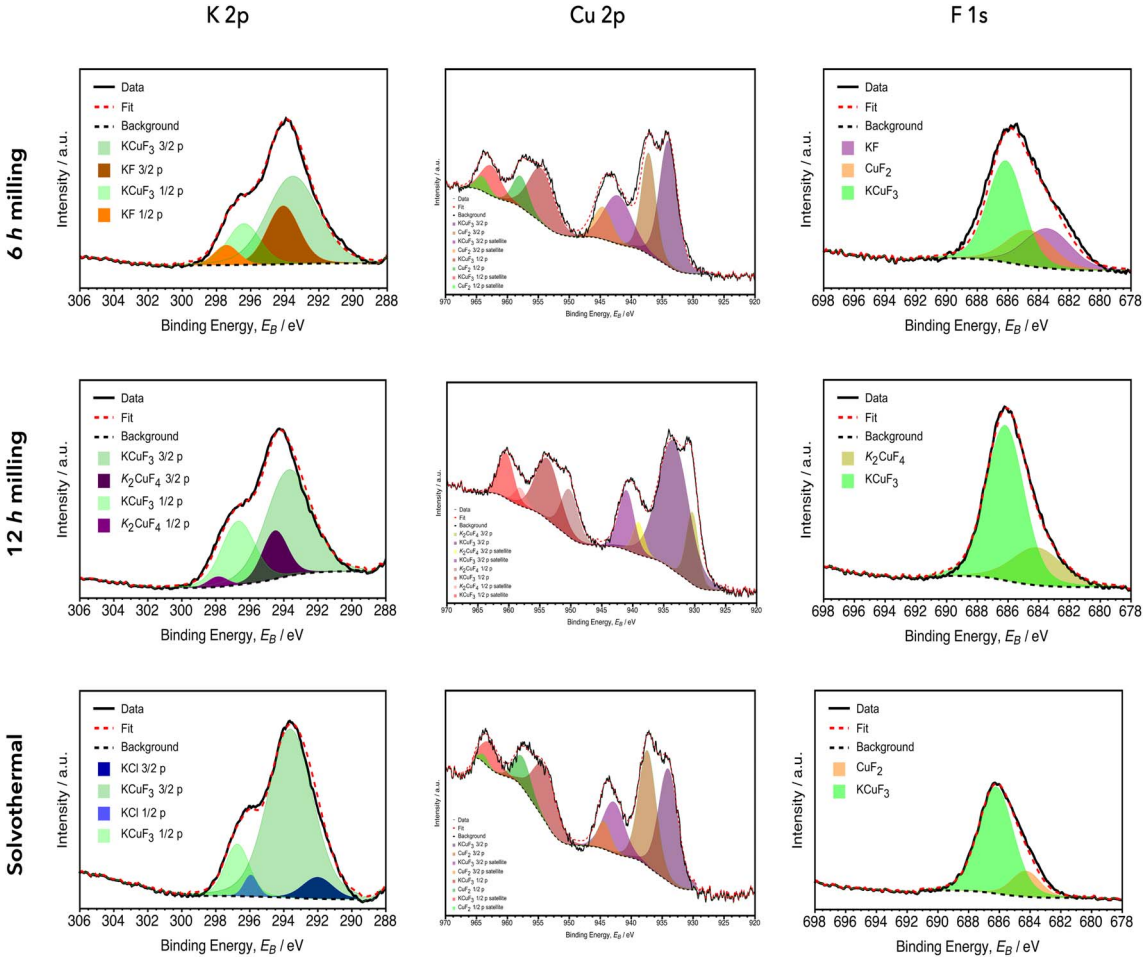

Fig. 4 Fitted K 2p, Cu 2p, and F 1s XPS high resolution spectra of $KCuF_3$ samples.

side peaks of KF at 292.3 ($2p_{3/2}$) and 295.1 eV ($2p_{1/2}$). In the XPS high resolution spectrum recorded for the sample synthesized by the 12 h mechanochemical process, in addition to the doublets of $KNiF_3$ at 293.5 ($2p_{3/2}$) and 296.4 eV ($2p_{1/2}$) and of KF at 292.1 eV ($2p_{3/2}$) and 294.8 eV ($2p_{1/2}$), another compound was detected: similar to what was observed in the copper-based perovskite, during the 12 h milling process a different perovskite characterized by the formula K_2NiF_4 was formed, as shown by the XRD data, and its doublet in the K 2p region can be ascribed to the contributions of the deconvolution detectable at 294.1 ($2p_{3/2}$) and 297.0 eV ($2p_{1/2}$). The binding energies of Ni $2p_{3/2}$ related to the $KNiF_3$ perovskite for all three analyzed samples were recorded at 858.1 ± 0.1 eV, corroborating the assignment of this peak to the perovskite product. Moreover, for the mechanochemical synthesis, an evident effect of milling time on the extent of reaction was observed: after 6 h, a slight amount of unreacted NiF_2 was still present and its signal at 860.4 eV was present together with that of the perovskite product; after 12 h, K_2NiF_4 started to be formed in addition to $KNiF_3$ and its signal was observable at 854.8 eV. In the sample produced by the solvothermal approach a peak at 856.1 eV was due to the excess of NiCl used as a reagent in the synthesis. In the F 1s high resolution spectra, sharp peaks ascribable to $KNiF_3$ were observed at 686.7 eV (±0.3 eV) in the 6 h and 12 milled samples as well as in the solvothermal sample, in agreement with the data reported in the literature.[11,42] The presence of other species, in addition to the perovskite product, detected by the analyses of the K 2p and Ni 2p signals, was also confirmed in the F 1s high resolution spectra. In particular, after 6 h two additional peaks due to an excess of KF and NiF_2 as

Table 7 Atomic composition by XPS analysis of $KNiF_3$ samples

Sample	Potassium at%	Nickel at%	Fluorine at%	Chlorine at%
6 h milling	25.5 (±0.3)	18.3 (±0.7)	56.2 (±0.6)	—
12 h milling	28.8 (±0.4)	14.1 (±0.5)	57.1 (±0.6)	—
Solvothermal	19.8 (±0.3)	18.4 (±0.7)	59.6 (±0.6)	2.2 (±0.02)

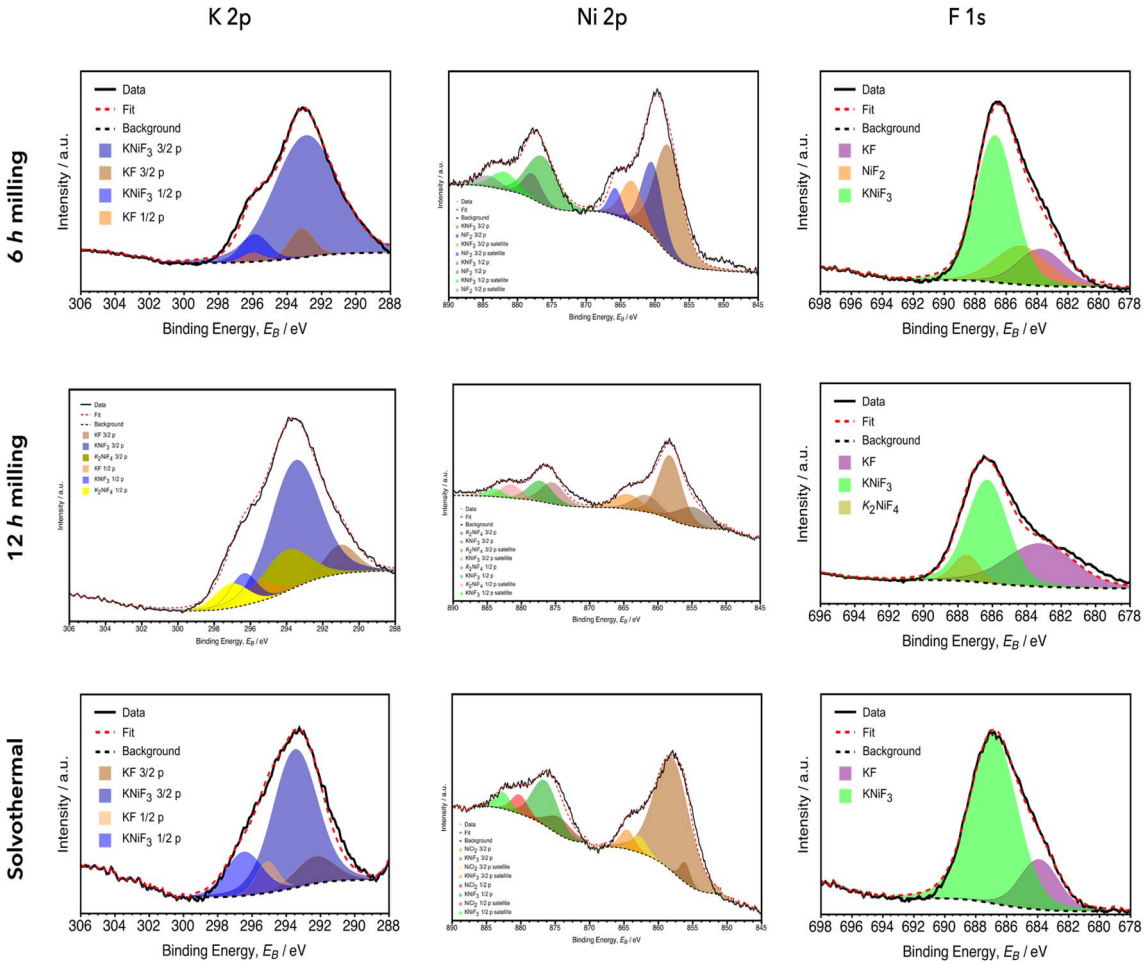

Fig. 5 Fitted K 2p, Ni 2p, and F 1s XPS high resolution spectra of $KNiF_3$ samples.

reagents were recorded at 683.7 eV and 685.2 eV, respectively. After 12 h it was also possible to notice both the presence of KF excess because of its signal at 683.3 eV and the formation of K_2NiF_4 due to its peak at 687.5 eV. In the F 1s spectrum of the solvothermal product, the $KNiF_3$ perovskite was the predominantly present species (around 80%) and the residual deconvoluted peak at 683.9 eV can be attributed to KF.

SEM results

The SEM images of $KCuF_3$ and $KNiF_3$ perovskites showed agglomerates that reached dimensions of 28 μm for $KCuF_3$ and 50 μm for $KNiF_3$ after a 3 h mechanochemical treatment, as reported in Fig. 6A and B, respectively. In both perovskites a gradual size reduction of bigger particles to approximately 17 μm with polydispersed granulometry was achieved by increasing the milling time to 6 and 12 h (Fig. 6C and D for $KCuF_3$ and $KNiF_3$ after 6 h and Fig. 6E and F for $KCuF_3$ and $KNiF_3$ after 12 h). Therefore, milling time was the key parameter for particle size reduction due to the collisions between particles and milling media. By means of the solvothermal approach, crystals of around 11 μm with a typical cubic shape, that is characteristic of ABX_3 perovskites, were clearly visible, as shown in Fig. 7A. Particles with similar size were formed with the mechanochemical method without the use of solvents or thermal treatment (Fig. 7B). However, as a result of aggregate breaking from the collisions with the milling media the cubic shape was scratched.

Green metrics and environmental impact

The environmental impacts of both solvothermal and mechanochemical methods were studied and compared through the use of green metrics. All the results obtained from the evaluation of the atom economy (AE), the theoretical process mass intensity (PMI) and the energy demand (ED) in the two processes are listed in Tables 8 and 9. All the details of the calculations of the green metrics and the energy assessment are reported in the ESI.†

The mechanochemical approach allowed the synthesis of the perovskites starting directly from fluoride salts, avoiding the use of chemicals which, even stoichiometrically, can produce side products; indeed, all the atoms of the reagents can be transformed into products. For the aforementioned reasons, the atom economy values of the samples obtained through the mechanochemical process were 100% and the corresponding values of PMI were 1. Although this conversion can be tempered by the reaction yield, the yields of mechanochemical processes

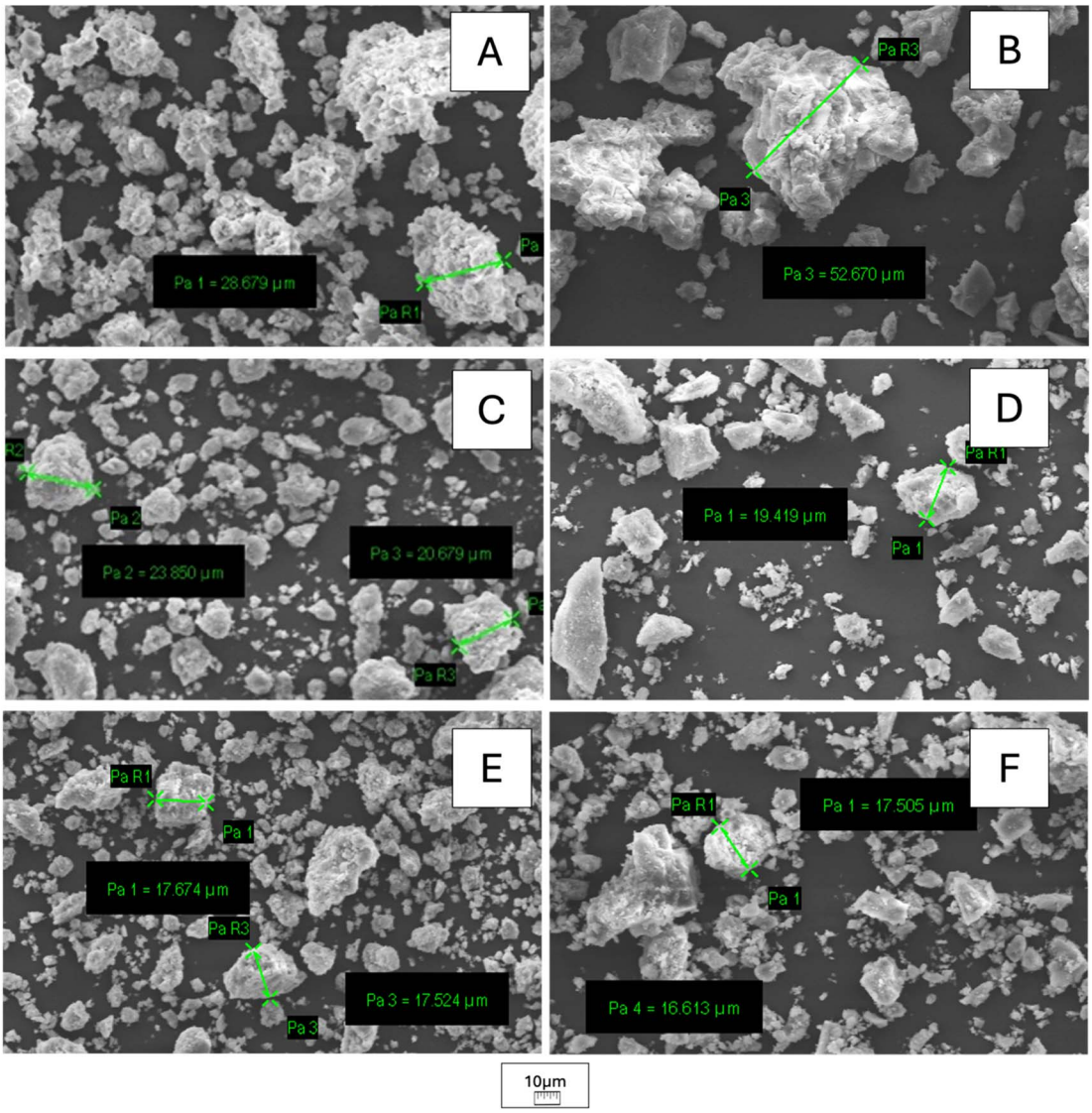

Fig. 6 SEM images of $KCuF_3$ (A–C) and $KNiF_3$ (D–F) perovskites obtained by mechanochemical solid-state synthesis at different milling times: after 3 h (A and D), 6 h (B and E) and 12 h (C and F), respectively.

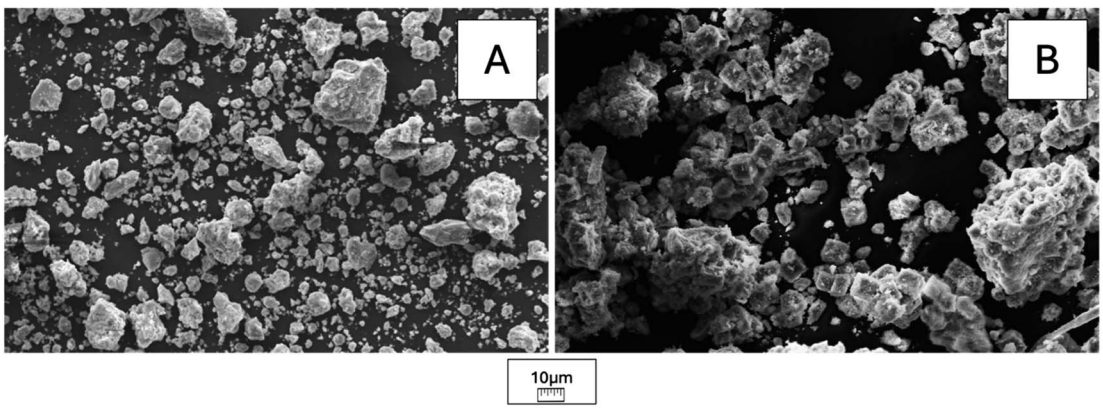

Fig. 7 SEM images of $KCuF_3$ perovskite obtained by mechanochemical solid-state synthesis after 6 h of milling time (A) as well as by solvothermal method (B).

Table 8 Green metrics evaluation for $KCuF_3$

Process	Milling time (h)	AE (%)	PMI (—)	ED (MJ g^{-1})
Mechanochemical	3	100%	1	0.58
	6	100%	1	1.16
	8	100%	1	2.32
Solvothermal	—	51.7%	191	6.1

Table 9 Green metrics evaluation for $KNiF_3$

Process	Milling time (h)	AE (%)	PMI (—)	ED (MJ g^{-1})
Mechanochemical	3	100%	1	0.58
	6	100%	1	1.16
	8	100%	1	2.32
Solvothermal	—	37.6%	294	9.5

are typically comparable to or higher than that of a solvothermal processes.

The green metrics of the solvothermal process considered the wastes caused by the use of chlorides in the synthesis of fluorinated perovskites, which necessarily lead to a higher consumption of potassium fluoride and to the formation of potassium chloride as a side product. It is possible to observe that the hydration water of the nickel chloride salt further reduces the atom economy leading to a final value of 37.6% for $KNiF_3$.

The energy demand was calculated for the mechanochemical process by considering the power of the ball miller employed and the different reaction times. The mechanochemical energy consumption was identical for both the perovskites because the optimized parameters were employed in both the syntheses and only the milling time was varied in the different samples. For the solvothermal synthesis, the heating time of the oven and the energy consumption during the synthesis and final drying step were considered.

On the basis of the energy assessment, the mechanochemical syntheses was clearly favourable from an energetic point of view because of the absence of waste of energy due to solvent heating, heat dispersion and final drying of the products. The dispersion of mechanical energy is therefore less impactful, especially for laboratory scale production. Overall, the mechanochemical process showed a clear advantage over the solvothermal process in the assessment of all the green metrics examined. All the details of the calculations are presented in the ESI.†

Conclusions

The fluorinated perovskites $KCuF_3$ and $KNiF_3$ were synthetized through a mechanochemical method and a new mild solvothermal process. In particular, the mechanochemical synthesis allowed the formation of $KCuF_3$ and $KNiF_3$ through a rapid and immediate process without the use of solvents. XRD and XPS characterization confirmed the formation of the desired crystalline phases, and the average size of the particles produced mechanochemically observed by SEM imaging was comparable with that of the solvothermal perovskites. The optimization of the mechanochemical syntheses, in terms of higher yields, greater selectivities of $KCuF_3$ and $KNiF_3$ perovskite products and best matching of crystalline dimensions compared to those of the solvothermal products, was obtained with a milling time of 6 h for both the chemical compounds. K_2CuF_4 and K_2NiF_4 crystalline phases were both observed to be formed after 12 h of mechanochemical syntheses. The environmental impacts of the mechanochemical and solvothermal syntheses were evaluated from both atomic and energetic point of views. The mechanochemical process was highly advantageous in terms of atom economy due to the absence of theoretical by-products and solvents in either the synthesis or the washing steps and because of the efficient use of raw materials. Mechanochemical synthesis was also preferable based on the energy demand, although the evaluations were limited to laboratory scale factors.

The absence of significant by-products and the ease of the mechanochemical process demonstrated that this kind of synthesis can be considered a valid alternative to the classic solvent-based approach. Thus, the described process can be extended to the synthesis of other fluorinated perovskites.

Data availability

The data supporting this article have been included as part of the ESI.†All the XPS surveys have been added as graphs as well as the original XRD spectra. All the calculations regarding the green metrics have been added in the apposite section. The SEM pictures are included in the original manuscript.

Conflicts of interest

There are no conflicts of interest to declare.

References

1 S. Sun, M. Lu, X. Gao, Z. Shi, X. Bai, W. W. Yu, *et al.*, 0D Perovskites: Unique Properties, Synthesis, and Their Applications, *Adv. Sci.*, 2021, **8**(24), 1–23.

2 X. Wang, Y. Peng, S. Yang, H. G. Yang and Y. Hou, Recent progress in metal halide perovskite photocatalysts for hydrogen evolution, *Mater. Chem. Front.*, 2023, **7**(20), 4635–4657. http://xlink.rsc.org/?DOI=D3QM00477E.

3 L. N. Quan, B. P. Rand, R. H. Friend, S. G. Mhaisalkar, T. W. Lee and E. H. Sargent, Perovskites for Next-Generation Optical Sources, *Chem. Rev.*, 2019, **119**(12), 7444–7477.

4 H. Peng, Y. H. Liu, X. Q. Huang, Q. Liu, Z. H. Yu, Z. X. Wang, *et al.*, Homochiral one-dimensional ABX 3 lead halide perovskites with high- T c quadratic nonlinear optical and dielectric switchings, *Mater. Chem. Front.*, 2021, **5**(12), 4756–4763. http://xlink.rsc.org/?DOI=D1QM00223F.

5 C. C. Stoumpos and M. G. Kanatzidis, The Renaissance of Halide Perovskites and Their Evolution as Emerging Semiconductors, *Acc. Chem. Res.*, 2015, **48**(10), 2791–2802.
6 E. Dagotto, Correlated electrons in high-temperature superconductors, *Rev. Mod. Phys.*, 1994, **66**(3), 763–840.
7 X. Tian, Z. Hu, Z. Gao, Y. Zhang, C. Li, H. Qi, *et al.*, Towards fluorinated Ruddlesden–Popper perovskites with enhanced physical properties: a study on (3-FC 6 H 4 CH 2 CH 2 NH 3) 2 PbI 4 single crystals, *Mater. Chem. Front.*, 2021, **5**(12), 4645–4657. **http://xlink.rsc.org/?DOI=D1QM00329A**.
8 R. A. H. Shakeel, S. Khan, A. Laref, G. Murtaza and J. Bila, Pressure induced physical variations in the lead free fluoropervoskites XYF3 (X=K, Rb, Ag; Y=Zn, Sr, Mg): Optical materials, *Opt. Mater.*, 2020, **109**, 110325. **https://linkinghub.elsevier.com/retrieve/pii/S0925346720306662**.
9 M. G. Hayatullah, R. Khenata, S. Muhammad, A. H. Reshak, K. M. Wong, *et al.*, Structural, chemical bonding, electronic and magnetic properties of KMF3 (M = Mn, Fe, Co, Ni) compounds, *Comput. Mater. Sci.*, 2014, **85**(221), 402–408, DOI: **10.1016/j.commatsci.2013.12.054**.
10 J. M. Ricart, R. Dovesi, C. Roetti and V. R. Saunders, Electronic and magnetic structure of KNiF3 perovskite, *Phys. Rev. B*, 1995, **52**(4), 2381–2389.
11 H. Fan, X. Zhang, Y. Wang, J. Lang and R. Gao, Highly conductive KNiF3@carbon nanotubes composite materials with cross-linked structure for high performance supercapacitor, *J. Power Sources*, 2020, **474**(February), 228603, DOI: **10.1016/j.jpowsour.2020.228603**.
12 H. Fan, X. Zhang, Y. Wang, R. Gao and J. Lang, Mn and Co co-doped perovskite fluorides KNiF3 with enhanced capacitive performance, *J. Colloid Interface Sci.*, 2019, **557**, 546–555, DOI: **10.1016/j.jcis.2019.09.051**.
13 M. Sturge *The Jahn-Teller Effect in Solids*. Solid stat. Academic Press; 1968. 91–211 p.
14 R. H. Buttner, E. N. Maslen and N. Spadaccini, Structure, electron density and thermal motion of KCuF3, *Acta Crystallogr., Sect. B: Struct. Sci.*, 1990, **46**(2), 131–138.
15 A. Okazaki and Y. Suemune, The Crystal Structure of KCuF 3, *J. Phys. Soc. Jpn.*, 1961, **16**(2), 176–183. **https://journals.jps.jp/doi/10.1143/JPSJ.16.176**.
16 Y. Huang, R. Ding, Q. Xu, W. Shi, D. Ying, Y. Huang, *et al.*, A conversion and pseudocapacitance-featuring cost-effective perovskite fluoride KCuF3for advanced lithium-ion capacitors and lithium-dual-ion batteries, *Dalton Trans.*, 2021, **50**(25), 8671–8675.
17 Y. Zhang, Y. Liu, J. Zhou, D. Wang, L. Tan and C. Yi, 3D cubic framework of fluoride perovskite SEI inducing uniform lithium deposition for air-stable and dendrite-free lithium metal anodes, *Chem. Eng. J.*, 2022, **431**(P3), 134266, DOI: **10.1016/j.cej.2021.134266**.
18 G. Dominiak-Dzik, I. Sokólska, S. Golab and M. Baluka, Preliminary report on growth, structure and optical properties of K5LaLi2F10:Ln3+ (Ln3+-Pr3+, Nd3+, Er3+) crystals, *J. Alloys Compd.*, 2000, **300**, 254–260.
19 K. Hirakawa, K. Hirakawa and T. Hasimoto, Magnetic Properties of Potassium Iron Group Fluorides KMF3, *J. Phys. Soc. Jpn.*, 1960, **15**(11), 2063–2068.
20 S. S-omiya, S. I. Hirano, M. Yoshimura and K. Yanagisawa, Hydrothermal crystal growth of perovskite-type fluorides, *J. Mater. Sci.*, 1981, **16**(3), 813–816.
21 R. Hua, Z. Jia and C. Shi, Preparation of KMgF3 and Eu-doped KMgF3 nanocrystals in water-in-oil microemulsions, *Mater. Res. Bull.*, 2007, **42**(2), 249–255.
22 F. Palazon, Y. El Ajjouri, P. Sebastia-Luna, S. Lauciello, L. Manna and H. J. Bolink, Mechanochemical synthesis of inorganic halide perovskites: evolution of phase-purity, morphology, and photoluminescence, *J. Mater. Chem. C*, 2019, **7**(37), 11406–11410. **https://xlink.rsc.org/?DOI=C9TC03778K**.
23 N. Leupold, K. Schötz, S. Cacovich, I. Bauer, M. Schultz, M. Daubinger, *et al.*, High Versatility and Stability of Mechanochemically Synthesized Halide Perovskite Powders for Optoelectronic Devices, *ACS Appl. Mater. Interfaces*, 2019, **11**(33), 30259–30268. **https://pubs.acs.org/doi/10.1021/acsami.9b09160**.
24 F. Palazon, Y. El Ajjouri and H. J. Bolink, Making by Grinding: Mechanochemistry Boosts the Development of Halide Perovskites and Other Multinary Metal Halides, *Adv. Energy Mater.*, 2020, **10**(13), 1902499. **https://onlinelibrary.wiley.com/doi/10.1002/aenm.201902499**.
25 P. A. Sukkurji, Y. Cui, S. Lee, K. Wang, R. Azmi, A. Sarkar, *et al.*, Mechanochemical synthesis of novel rutile-type high entropy fluorides for electrocatalysis, *J. Mater. Chem. A*, 2021, **9**(14), 8998–9009. **https://xlink.rsc.org/?DOI=D0TA10209A**.
26 Y. Chen, W. Li, X. H. Wang, R. Z. Gao, A. N. Tang and D. M. Kong, Green synthesis of covalent organic frameworks based on reaction media, *Mater. Chem. Front.*, 2021, **5**(3), 1253–1267. **http://xlink.rsc.org/?DOI=D0QM00801J**.
27 P. Dulian, W. Bąk, K. Wieczorek-Ciurowa and C. Kajtoch, Controlled mechanochemical synthesis and properties of a selected perovskite-type electroceramics, *Mater. Sci.*, 2013, **31**(3), 462–470. **http://link.springer.com/10.2478/s13536-013-0126-4**.
28 L. Martínez-Sarti, F. Palazon, M. Sessolo and H. J. Bolink, Dry Mechanochemical Synthesis of Highly Luminescent, Blue and Green Hybrid Perovskite Solids, *Adv. Opt. Mater.*, 2020, **8**(4), 1901494. **https://onlinelibrary.wiley.com/doi/10.1002/adom.201901494**.
29 X. Su, N. Li, K. Wang, Q. Li, W. Shao, L. Liu, *et al.*, Real time optical monitoring of cascade mechanochemical reactions and capture of ultra-unstable intermediates under hydrostatic pressure, *Mater. Chem. Front.*, 2023, **7**(18), 4040–4049. **http://xlink.rsc.org/?DOI=D3QM00282A**.
30 N. Fantozzi, J. N. Volle, A. Porcheddu, D. Virieux, F. García and E. Colacino, Green metrics in mechanochemistry, *Chem. Soc. Rev.*, 2023, **52**(19), 6680–6714. **https://xlink.rsc.org/?DOI=D2CS00997H**.
31 P. T. Anastas and J. C. Warner. *Green Chemistry*. Oxford University PressOxford; 2000. **https://academic.oup.com/book/53104**.
32 V. K. Singh, A. Chamberlain-Clay, H. C. Ong, F. León, G. Hum, M. Y. Par, *et al.*, Multigram Mechanochemical

synthesis of a Salophen Complex: A Comparative Analysis, *ACS Sustain. Chem. Eng.*, 2021, **9**(3), 1152–1160. **https://pubs.acs.org/doi/10.1021/acssuschemeng.0c06374**.

33 C. F. Burmeister, M. Hofer, P. Molaiyan, P. Michalowski and A. Kwade, Characterization of Stressing Conditions in a High Energy Ball Mill by Discrete Element Simulations, *Processes*, 2022, **10**(4), 692.

34 R. Schlem, C. F. Burmeister, P. Michalowski, S. Ohno, G. F. Dewald, A. Kwade, *et al.*, Energy Storage Materials for Solid-State Batteries: Design by Mechanochemistry, *Adv. Energy Mater.*, 2021, **11**(30), 2101022.

35 P. Scherrer and P. Debye, Scherrer equation, *Physik*, 1916, **17**, 277–283.

36 C. Burmeister, L. Titscher, S. Breitung-Faes and A. Kwade, Dry grinding in planetary ball mills: Evaluation of a stressing model, *Adv. Powder Technol.*, 2018, **29**(1), 191–201. **https://linkinghub.elsevier.com/retrieve/pii/S0921883117304223**.

37 N. Tyagi, E. Ghanti, N. Gupta, N. P. Lalla and R. Nagarajan, Synthesis of nanocrystalline mixed metal fluorides in nonaqueous medium, *Bull. Mater. Sci.*, 2009, **32**(6), 583–587.

38 D. Briggs and M. P. Seah. *Practical Surface Analysis*. 2nd edn John Wiley & Sons, Ltd; 1993, vol. 1 & 2.

39 B. E. Chenhall, J. Ellis, P. T. Crisp, R. Payling, R. K. Tandon and R. S. Baker, Application of surface science, *Appl. Surf. Sci.*, 1985, **20**, 527–537.

40 V. I. Nefedov, D. Gatin, B. F. Dzhurinskii, N. P. Sergushin and Y. V. Salyn', X-ray electron investigations of some element oxides, *Russ. J. Inorg. Chem.*, 1975, **20**, 2307–2314.

41 J. F. Moulder, W. F. Stickle, P. E. Sobol and K. D. Bomben. *Handbook of X-Ray Photoelectron Spectroscopy*. Perking-Elmer Corporation. 2005. 621–622 p.

42 M. Zhang, Z. Wang, M. Mo, X. Chen, R. Zhang, W. Yu, *et al.*, A simple approach to synthesize KNiF3 hollow spheres by solvothermal method, *Mater. Chem. Phys.*, 2005, **89**(2–3), 373–378.

43 **https://www.lasurface.com**.